Critical factors in 3D model reconstruction using the Roofer algorithm: an analysis of geometric and topological consistency in mountainous cities

Gizela Guzmán Lugo[1], Iván Lizarazo Salcedo[1], Camilo León Sánchez[2]

[1] Universidad Nacional de Colombia, Faculty of Agricultural Sciences, Bogotá, Colombia.
{gguzmanl,ializarazos}@unal.edu.co
[2] Laboratory of Geo-information Science and Remote Sensing, Wageningen University & Research, Gelderland, Wageningen, 6700 AA, The Netherlands. camilo.leonsanchez@wur.nl

Keywords: 3D reconstruction, Roofer, s3DCM, geometric validation, quality control, Urban Digital Twins

Abstract

Semantic 3D city models (s3DCM) are a key component of urban digital twins (UDT) because they integrate geometry and semantic information in three-dimensional environments. However, generating geometrically consistent and interoperable models remains challenging due to data heterogeneity and the sensitivity of the reconstruction processes. This research identifies and analyzes the critical factors that influence the quality of s3DCM in the Colombian context of mountainous cities, while also developing a methodological workflow based on the Roofer algorithm for LoD2 reconstruction to generate energy-oriented UDT by integrating building footprints and lidar data. The results show that footprint quality and consistency, together with lidar classification, are the main determinants of 3D reconstruction accuracy. In addition, mountainous terrain and local construction practices require further adjustments of the algorithm parameters that better reflect real-world conditions. Multiple adjustments to the input data and algorithm parameters show that model quality depends on rigorous preprocessing, appropriate geometric validation, and, in mountainous areas, accurate estimation of building base height. Finally, we propose a reproducible workflow for s3DCM generation based on the identified critical factors. The workflow provides a foundation for urban analysis and an energy-oriented UDT implementation in mountainous cities.

1. Introduction

Urban development increasingly requires innovative solutions to address the complex dynamics of contemporary urban environments. In this context, the concept of Urban Digital Twin (UDT) has emerged as a platform for simulating and analyzing urban scenes, improving understanding of how cities function, evaluating the effects of different management strategies, and supporting decision-making (Luo et al., 2025).

A fundamental component of a UDT is the semantic 3D city model (s3DCM), which integrates the geometry and semantic information of urban objects within a three-dimensional environment (León Sánchez, 2025), enabling analyses such as energy, mobility, or noise (Alvi et al., 2025). The storage and management of s3DCM is normally based on the OGC CityGML standard (Gröger et al., 2012), which integrates geometric, semantic, and functional information about buildings and supports simulations of the physical behavior of the urban environment (Bing-Shiuan, 2024).

CityGML organizes the geometric and semantic representation of urban objects into Levels of Detail (LoD), which define the degree of accuracy and complexity with which an element is modeled. This structure supports different analysis scales while maintaining coherence between representations (OGC, 2021) (OGC, 2021). Our research focuses on LoD2, which enables a realistic yet generalized representation of roofs (see figure 1), suitable for rooftop solar potential analysis, where geometric fidelity and shading accuracy are essential.

Several studies have evaluated the quality of CityGML data and confirmed that geometric and semantic errors are common even in models already structured according to the standard.

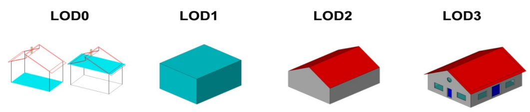

Figure 1. Representation of detail levels 0–3. Source: (OGC, 2021).

Biljecki et al. (2016), after analyzing 37 CityGML datasets, report that completely error-free models are uncommon; typical errors include invalid geometries, improper intersections, non-closed volumes, and semantic inconsistencies. These findings highlight the need to incorporate rigorous geometric and topological validation to ensure that the models are usable for simulations and analyses.

Despite various efforts to validate 3D models—primarily focused on geometric and topological coherence (Wysocki et al., 2024; Lei et al., 2023)—these approaches still lack an integrated framework to assess quality, usability, and suitability for specific applications (Lei et al., 2023). Consequently, a significant gap remains in evaluating how closely the 3D models reflect reality and which factors affect the quality of the 3D reconstruction.

Although there are various methods for the automatic reconstruction of s3DCM, most assume that the input data meet the required geometric and topological criteria. However, in countries such as Colombia, official geospatial products were developed for cartographic and cadastral purposes, not for the automatic reconstruction of 3D models. Consequently, uncertainty remains regarding the suitability of these inputs for LoD2 processes and how their quality—along with the mountainous terrain and urban morphological heterogeneity—affects the quality of the models.

https://doi.org/10.5194/isprs-annals-XII-4-W2-2026-57-2026

This research addresses the following question: What are the critical factors affecting the generation of geometrically consistent and topologically valid s3DCM from the available geospatial datasets in Colombia's mountainous cities? To answer it, we propose an iterative experimental design that systematically evaluates the influence of input-data quality, preprocessing strategies, terrain conditions, and reconstruction parameters on LoD2 building generation. Our research uses Roofer as the reconstruction algorithm, which has good performance in LoD2 benchmarks in terms of robustness and efficiency (Geniet et al., 2025) and supports large-scale study areas such as the Dutch 3DBAG (Peters et al., 2022). This research identifies the key determinants of geometric consistency and topological validity, and it establishes a reproducible workflow tailored to the Colombian context.

2. Data and Methods

2.1 Study Area

This research is conducted in the urban area of Tunja municipality, the capital of the Boyacá department, located in the central Andean region of Colombia. The city lies at a mean altitude of 2782 m above sea level, with elevations ranging from 2,672 to 2,970 m above sea level. Characterizing an urban environment with a mountainous relief and steep slopes. The study area exhibits morphological heterogeneity, characterized by attached and detached buildings, irregular building footprints, diverse roof typologies and construction materials, and locally varying building base elevations associated with the mountainous terrain, resulting in an architecturally and geometrically irregular urban fabric. The study area covers 100 ha and comprises 66 urban blocks. However, to ensure the identification of critical factors, the analyses presented in this paper focus on five urban blocks. These blocks exhibit heterogeneous characteristics and were selected based on their construction typology, morphological configuration, and urban composition (see figure 2).

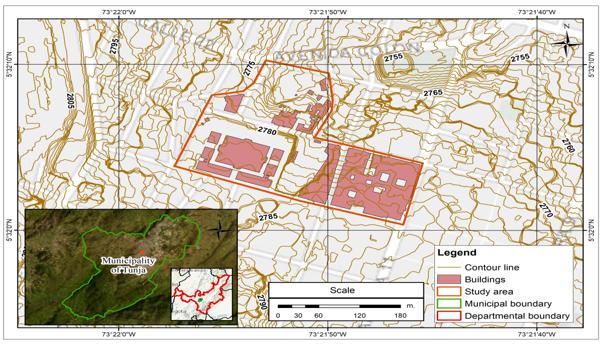

Figure 2. Study area

2.2 Data

The data were obtained from official national sources and aerial surveys conducted between 2018 and 2022 (see table 1).

Data type	Year	Resolution / Density	Format	Main use
lidar point cloud	2022	4–8 pts/m^2	LAS	3D modelling
Digital Terrain Model (DTM)	2022	1 m	TIF	Building base level
Building footprints (IGAC)	2022	Scale 1:1,000	GDB	Spatial delimitation of buildings
Building footprints (Cadastre)	2018	Scale 1:25,000	SHP	Spatial delimitation of buildings
Orthophoto	2022	0.1 m	TIF	Visual inspection

Table 1. Data characteristics.

2.3 Methods

First, the s3DCM is generated using Roofer's default configuration. The resulting model is then analyzed through geometric and topological validation and visual inspection. Based on the identified errors, the patterns underlying their occurrence are examined, including input data quality, environmental factors, and the algorithm's sensitivity to parameter settings. This setup enables a systematic evaluation of how different reconstruction configurations affect the model's quality and provides a reproducible basis for comparison.

2.3.1 Verification and preparation of input data: This process aims to verify that the inputs used for the 3D reconstruction meet the minimum processing requirements. First, the basic properties of the input data are checked, including format, spatial coverage, data integrity, and consistency across sources. The spatial reference system is then verified and, where necessary, adjusted to ensure alignment between the lidar point cloud and the building footprints. This harmonization is essential to avoid displacement and geometric mismatch.

2.3.2 Algorithm parameter setting: The s3DCM reconstruction algorithm supports parameter configuration across three categories: input options (which define footprint attributes and filtering criteria), clipping options (which control preprocessing of lidar point-cloud subsets, including geometry simplification and point-density limits), and reconstruction options (which determine the algorithm's behavior during 3D model generation).

This research analyzes Roofer parameters across these three categories, such as the `h-terrain-attribute` (terrain height fallback), `ceil-point-density` (maximum point density per building), `complexity-factor` (level of detail), `clip-terrain` (roof delimitation through the trimming of ground points), `plane-detect-k` (number of neighbors), and `plane-detect-epsilon` (fitting tolerance). In the first iteration ($i = 0$), the algorithm is executed with the default parameters. In subsequent iterations ($i = n$), the parameters are adjusted based on critical factors. These adjustments are evaluated iteratively until a configuration is reached that optimizes geometric quality and topological validity.

2.3.3 3D Reconstruction: The algorithm consists of six stages: (1) roof-plane detection through region-growing segmentation; (2) determination of structural lines from intersections between planes and segment boundaries; (3) grouping and regularization of these lines according to orientation and spatial proximity; (4) generation of an initial roof partition; (5) optimization of this partition using a graph-cut algorithm that assigns to each region the plane that best fits the data; and (6) extrusion of the optimized partition to obtain a closed 3D model representing the general shape of the building (Peters et al., 2022).

2.3.4 Geometric and topological consistency assessment: The quality of the model is evaluated using a set of metrics that assess geometric consistency, topological validity, and structural coherence. This evaluation enables identification of the types of errors in the reconstructed models and their relationship to the methodological decisions applied during the reconstruction process.

Topological consistency: Evaluated using `val3dity` (Ledoux, 2018), which verifies compliance with the geometric rules defined in the ISO 19107 standard for three-dimensional solids. This process enables the identification of critical errors, such as self-intersections, holes in the solid, and incorrect orientations, which affect the topological integrity of the model.

Geometric consistency: Two complementary metrics are used. The Hausdorff distance measures the maximum discrepancy between the input building's footprint and the reconstructed footprint, capturing the greatest spatial deviation between the two geometries (Taha and Hanbury, 2015). The IoU metric quantifies the degree of surface overlap between the compared polygons and reflects their spatial agreement in terms of area (Zhou et al., 2019).

The Hausdorff distance (H) between two point sets A and B is the maximum of the distances between each point in A and its nearest neighbor in B, where $\|x - y\|$ represents a (Euclidean) distance function.

$$H(A, B) = \max_{x \in A} \left\{ \min_{y \in B} \|x - y\| \right\} \tag{1}$$

IoU is defined as:

$$IoU = \frac{G \cap R}{G \cup R} \tag{2}$$

Where G is the reference geometry and R is the reconstructed geometry.

Metric accuracy: The degree of fit between the reconstructed model and the original lidar data is evaluated by calculating the Root Mean Square Error (RMSE) of the vertical distance between lidar points and model surfaces:

$$RMSE = \sqrt{\frac{1}{n} \sum_{i=1}^{n} (Z_{\mathrm{mod},i} - Z_{\mathrm{lidar},i})^2} \tag{3}$$

where Z_{mod} is the roof elevation of the 3D model and Z_{lidar} is the roof elevation derived from lidar.

Quantitative evaluation of algorithm performance: Output attributes for each building are analyzed, including modeling success (extrusion mode), vertical coherence (floor elevation and maximum roof height), data quality (no-data fraction and point density within the footprint), and geometric consistency (volume).

Visual and consistency assessment of the model: A systematic visual assessment is conducted to verify the structural consistency of the model and its precision in reflecting the real morphology of the buildings. This ensures that the architectural layout of the urban environment is represented logically and realistically.

2.3.5 Identification of critical factors: Based on the comparative analysis of the generated models and detected errors, recurring patterns are identified and linked to specific methodological decisions. Through an inductive approach, factors are recognized, including footprint inconsistencies, Z-coordinate issues, internal building delineation, lidar classification quality, vegetation, misalignment between data sources, base elevation estimation in sloped areas, and architectural features. Progressive adjustments are then applied to determine whether identified issues can be addressed through Roofer parameter optimization or require preprocessing of the input data. This approach isolates the effect of each factor, generating comparable models with traceable configurations to assess their impact on geometric and topological consistency.

2.3.6 Refinement of input data: This process includes interventions on footprints, such as topological validation, correction of invalid geometries, and 2D standardization by removing height values. The lidar point cloud includes filtering for relevant classes (ground and buildings), reclassifying erroneous points, removing ground points within footprints, and estimating base elevation (Z_0).

2.3.7 Methodological workflow design: Finally, a structured workflow is consolidated to organize the stages required to generate consistent and interoperable 3D models from lidar data in urban contexts with complex topography. The resulting workflow identifies the critical factors in the process, the required quality controls, and the methodological adjustments that reduce the occurrence of geometric and topological errors, thereby constituting a reproducible guide for 3D urban model reconstruction in the Colombian context.

3. Results

This section presents the results of the analyses structured around the critical factors identified during the reconstruction process. These factors can be grouped into two main categories: (i) the quality and coherence of the input data (factors 1, 2, 3, 4, and 5) and (ii) the physical and constructive conditions of the urban environment (factors 6, 7, 8, and 9). For each factor, a specific analysis is provided, supported by metrics and figures that illustrate the effects observed during the evaluation phase. These elements were selected for their ability to clearly show the model's behavior with respect to each analyzed factor. Detailed documentation of the factors is available in *GitHub repository*.

3.1 Critical factor 1: Geometric inconsistencies in footprints

During the first Roofer iteration, geometric errors were detected in the building footprints provided by the Colombian Geographic Institute (IGAC), which prevented the algorithm from executing and, consequently, from generating the 3D reconstruction. Although these footprints were valid for 2D environments and complied with cartographic standards, they contained inconsistencies such as self-intersections and nested inner rings, thereby violating the rules defined by the OGC Simple Feature Access standard (OGC, 2021). To address this issue, the footprints were checked and corrected using the geometry validation tools available in QGIS (*Check Validity Fix Geometries*), complemented by manual editing in specific cases (Kukulska et al., 2018). This correction process ensured the geometric validity of the footprints and enabled the proper execution of Roofer. figure 3 illustrates the geometric inconsistencies identified in the original input data.

https://doi.org/10.5194/isprs-annals-XII-4-W2-2026-57-2026 | © Author(s) 2026. CC BY 4.0 License.

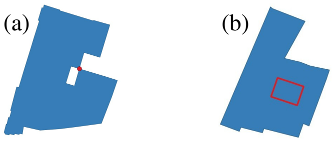

Figure 3. Geometric errors in the input data. (a) Self-intersection; (b) Nested inner rings.

3.2 Critical factor 2: Footprints with 3D information

The presence of 3D information in building footprints introduced geometric inconsistencies. Specifically, when IGAC footprints containing vertex-level Z coordinates were used, invalid surfaces emerged in the reconstructed model. In addition, simplified footprint outlines—i.e., outlines that do not follow the actual building geometry from vertex to vertex—were identified as an inherent consequence of the photogrammetric restitution process. These outlines, together with noncoplanar vertex elevations, hindered the generation of planar surfaces during reconstruction.

To assess the impact of this condition, comparative reconstructions were performed using two input configurations: (i) footprints with the original 3D information, (ii) 2D footprints obtained by removing the Z component. Table 2 summarizes the geometric metrics obtained for the two evaluated footprint configurations.

Config.	% Failed extrusions	RMSE (m)	% Invalid Solid	% Invalid MultiSurface	Volume (m^3)	Hausdorff dist. (m)	IoU
i	25.0%	0.23	20.0%	75.0%	17770.57	5.824	0.93
ii	25.0%	0.23	20.0%	0.0%	17917.33	5.826	0.93

Table 2. Comparison of geometric and topological metrics for different building footprint configurations.

Topological validation of the Multi-surfaces revealed that configuration (i) produced approximately 75% invalid Multi-surfaces, while no invalid cases were identified for the 2D footprints. These results demonstrate that inconsistent Z coordinates affect the surface quality of the model (faces), although they do not necessarily impact the overall volumetric representation (solid).

3.3 Critical factor 3: Inconsistent internal buildings

When an alternative cadastral layer was used as input, geometric errors emerged in the reconstructed models in the form of "table-leg" artifacts. These errors do not stem from the reconstruction parameters or the lidar classification, but rather from inconsistencies in the internal delineation of buildings. In this dataset, a single construction was represented by partial subdivisions and internal polygons that did not constitute complete footprints. Such internal delimitation lacks surrounding terrain points, preventing the algorithm from correctly identifying the base surface and resulting in anomalous extrusions.

To solve this issue, the internal polygons were merged into a single, continuous footprint for each building. After this adjustment, the "table-leg" artifacts disappeared, resulting in geometrically coherent models. As illustrated in figure 4, the model generated from the original configuration is shown in green, while the adjusted model is shown in orange. Table 3 presents the geometric metrics obtained for both scenarios.

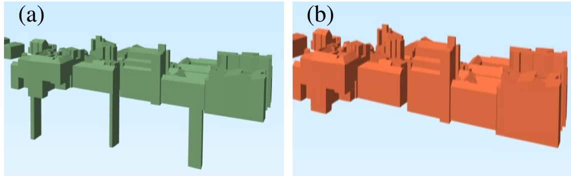

Figure 4. Geometric effect of internal footprint subdivision: (a) Original footprints; (b) Unified footprints.

A decrease in volume is observed after the removal of the "table-leg" artifacts present in the original model, reflecting an approximate difference of 26 m in base elevation. Likewise, a slight increase in RMSE is detected, associated with error propagation introduced during the unification process, without significant deterioration in geometric fit.

Footprint type	h_{ground} **(m)**	h_{roof} **(m)**	**RMSE (m)**	**Volume (m^3)**
Original	2775.53	2793.40	0.40	2221.53
Adjusted	2781.83	2797.06	0.42	1639.28

Table 3. Comparison of metrics for footprints with internal subdivisions and unified footprints.

3.4 Critical factor 4: Quality of lidar classification

Incorrect classification of the lidar point cloud, particularly within the building class, reduces Roofer's ability to detect roof planes, especially in roof-intersection zones. These misclassifications led to detection failures, partial reconstructions, non-extruded elements, and topological errors such as consecutive identical points and non-manifold cases, which were substantially reduced after refining the classification.

Additionally, the `clip-terrain` parameter was disabled to avoid terrain-induced clipping of reconstructed buildings resulting from the presence of ground points within or at the edges of building footprints. To evaluate the impact of lidar classification refinement and parameter adjustment, the results obtained from the original, refined, and refined + no-clip terrain configurations were compared. Table 4 presents the geometric metrics derived from these configurations.

Lidar	**% Failed extrusion**	h_{ground} **(m)**	h_{roof} **(m)**	**RMSE (m)**
Original	0.12%	2776.32	2787.53	0.44
Refined	0.01%	2776.50	2786.68	0.29
Refined + no-clip terrain	0.01%	2776.50	2786.68	0.29
Lidar	**% Invalid val3dity**	**Volume (m^3)**	**Hausdorff dist. (m)**	**IoU**
Original	0.06%	3434.33	1.57	0.96
Refined	0.01%	3074.56	0.55	0.99
Refined + no-clip terrain	0.01%	3142.35	0.070	≈ 1.00

Table 4. Comparison of lidar classification refinement metrics.

Table 4 shows that refining the LiDAR classification improved the geometric and topological quality of the reconstructed models, with improvements across all evaluated metrics. Adjusting the clip-terrain parameter improved topological consistency and planimetric agreement between the reconstructed footprints and the reference footprints by preventing the geometry from being clipped by terrain points, resulting in an IoU of approximately 1.0.

figure 5 shows differences between reconstructions from the original and refined LiDAR point clouds, including classification inconsistencies and improved geometric definition after refinement.

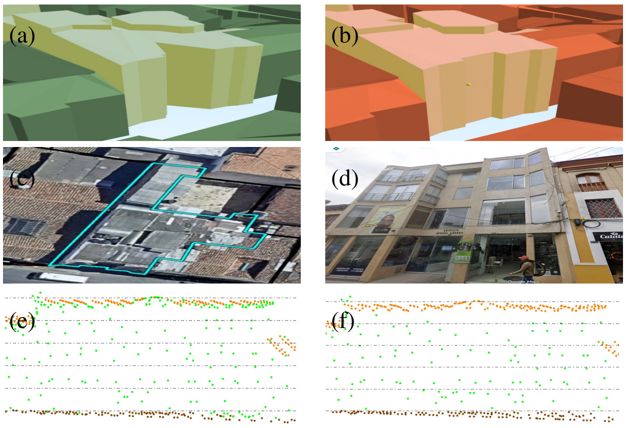

Figure 5. Effect of lidar classification. (a) Original lidar model; (b) Refined lidar model; (c) Orthoimage; (d) Reference image; (e) Original lidar profile; (f) Refined lidar profile.

3.5 Critical factor 5: Misalignment between footprints and lidar

IGAC footprints represent entire blocks rather than individual buildings; therefore, they had to be subdivided through visual interpretation. As a result of this process, spatial misalignments were introduced that affected the 3D reconstruction, since the outlines of some buildings did not exactly match the lidar point cloud, resulting in inconsistencies such as buildings with partial volume loss due to overlap between their footprints and those of their surroundings. When using the footprint as a boundary to clip the lidar point cloud, the algorithm incorrectly incorporates points from the adjacent building, leading to incorrect roof-plane estimation and the generation of inconsistent volumes with artificial vertical faces.

In addition, inaccurate volumetric reconstructions resulting from this misalignment were identified. In particular, when lidar points from a taller neighboring building were included within the footprint, the algorithm reconstructed a volume that did not correspond to the actual building. To evaluate the impact of this critical factor, the reconstructions obtained using the original and adjusted footprints were compared. table 5 presents the metrics for both scenarios.

Error	Footprint type	h_{ground} (m)	h_{roof} (m)	RMSE (m)	Volume (m^3)
Displaced volume	Original	2780.81	2799.65	0.88	6363.28
	Adjusted	2780.81	2799.65	0.96	5945.81
False reconstruction	Original	2772.35	2791.40	2.30	1886.49
	Adjusted	2772.33	2783.42	0.10	1418.62

Table 5. Comparison of footprint misalignment metrics.

In the first case, the differences are reflected mainly in the volume, and in the other case, the RMSE decreases because the model aligns with the point cloud, producing volumes that are more consistent with the building's actual morphology. It should be noted that these correspond to two individual case studies and are therefore presented as illustrative examples of the impact of correcting significant footprint errors, rather than as average improvements across the entire dataset. This factor demonstrates that the positional quality of the footprints is a key condition for the geometric validity of the reconstructed model. figure 6 illustrates how footprint correction eliminates volumetric distortions and improves the spatial coherence of the model.

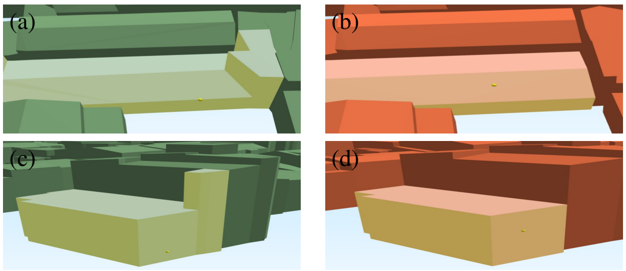

Figure 6. Effect of footprint misalignment. (a) Displaced volume error; (b) Displaced volume adjustment; (c) False reconstruction error; (d) False reconstruction adjustment.

3.6 Critical factor 6: Presence of vegetation

A single building, representing 0.01%of the cases reported in table 4, could not be extruded; this was attributed to surrounding vegetation, which caused occlusion during lidar acquisition and reduced the effective point density over the rooftops. This limited the availability of information in key areas, affecting plane detection and Roofer's ability to perform the reconstruction. To verify whether the issue could be resolved through algorithm configuration, several parameters were adjusted: `plane-detect-min-points` (from 15 to 10 and 5), `ceil-point-density` (from 20 to 30), and `plane-detect-k` (increasing the number of neighbors), but extrusion was still not achieved. This behavior suggests that the limitation was not parametric but instead resulted from the absence of roof points due to vegetation-induced occlusion.

3.7 Critical factor 7: Base elevation estimation in sloped areas

In s3DCM located on steep slopes (characterized by stepped buildings, partially buried structures, or retaining walls), inconsistencies were identified regarding the estimation of the base elevation (Z_0), which Roofer calculates using the 5th percentile of terrain points within a 3m buffer around the footprint. However, in sloped contexts, significant variations in ground elevation can result in inaccurate Z_0 values, causing the model to be anchored to a single elevation that does not correspond to the actual base elevation.

To assess this behavior, a Python script was implemented to compute Z_0 using a reduced buffer of 1m, which was incorporated as an input attribute. This reduced the influence of terrain points located farther from the actual base and improved the estimation of the base level. Three representative buildings (ID 21, 54, and 55) were evaluated, and table 6, presents the difference between the estimated base elevation and the DTM elevation.

ID cons	Footprint type	h_{ground} (m)	h_{roof} (m)	RMSE (m)	Volume (m^3)	Diff(m) vs DTM
21	Original	2777.06	2793.29	0.51	3673.27	3.24
	Adjusted	2780.12	2793.29	0.51	2715.05	**0.18**
54	Original	2775.80	2781.41	0.34	382.72	1.60
	Adjusted	2777.00	2781.41	0.34	285.73	**0.41**
55	Original	2771.57	2780.43	0.14	2081.13	4.78
	Adjusted	2774.73	2780.43	0.14	1199.16	**1.61**

Table 6. Comparison of metrics for estimating base elevation.

The results indicate a substantial reduction in the difference between the estimated base elevation and the DTM, reflecting an improvement in the accuracy of the base elevation. In contrast, metrics such as RMSE and roof heights remain practically constant, meaning that the adjustment does not affect roof reconstruction, but specifically the definition of the base level. Figure 7 presents a visual comparison between the original model (green) and the model with recalculated Z_0 (orange), together with facade images and elevation profiles highlighting the characteristic elevation variability of sloped areas.

Figure 7 compares the original model (green) and the model with the recalculated Z_0 value (orange), together with facade images and elevation profiles highlighting the characteristic elevation variability of sloped areas.

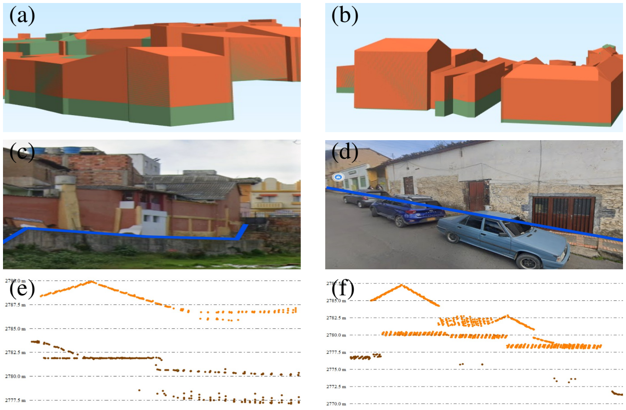

Figure 7. Effect of base elevation estimation in sloped areas. (a)–(b) 3D models with Z_0 adjustment; (c)–(d) reference images; (e)–(f) lidar profiles.

3.8 Critical factor 8: Polycarbonate roofs

In buildings with roofs composed of translucent materials (such as polycarbonate), the lidar signal can penetrate the structure, generating returns from both the roof and the ground. These returns beneath the roof are incorrectly classified as ground points, leading Roofer to interpret them as open surfaces or inner courtyards and thereby producing artificial voids or cavities in the reconstructed volume. To address this issue, two strategies were implemented: (1) refinement of lidar data by removing ground-classified points beneath translucent roofs; and (2) adjustment of the `clip-terrain` parameter to `false`, preventing automatic roof clipping when ground patches are detected. Both approaches yielded equivalent results and allowed the correct reconstruction of roof geometry. Figure 8 illustrates an example of this behavior.

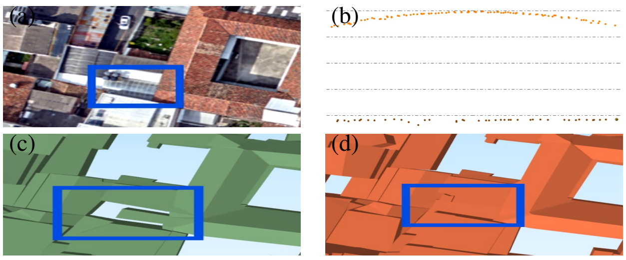

Figure 8. Effect of polycarbonate roofing. (a) Reference image; (b) LiDAR profile; (c) Original 3D model; (d) Adjusted 3D model.

Table 7 compares the geometric metrics of a reference building before and after the adjustments. Improvements in Hausdorff distance and IoU indicate greater geometric correspondence between the reconstructed model and the reference.

Footprint type	h_{ground} (m)	h_{roof} (m)	RMSE (m)	Volume (m^3)	Hausdorff dist.(m)	IoU
Original	2778.40	2790.57	0.42	28192.20	6.38	0.98
Adjusted	2778.38	2790.56	0.43	28861.11	0.71	1.00

Table 7. Comparison of metrics for polycarbonate roof adjustment.

3.9 Critical factor 9: Local construction characteristics

Limitations were identified in the representation of buildings with protruding architectural elements (overhangs, balconies, parapets, and rooftop water tanks). In some cases, these surfaces are artificially projected to the ground, generating unrealistic vertical faces; in other cases, they are omitted entirely, resulting in a simplified representation that affects the derived analyzes. Figure 9 illustrates some of these cases.

Figure 9. Examples of local architectural features.

For solar potential estimation, rooftop water tanks are relevant because they occupy usable surface area and generate shadows. Tests were conducted to reconstruct these elements using available lidar data; however, several limitations were identified. First, automatic classification algorithms do not recognize these objects as distinct classes. Second, the point density over these elements is insufficient for the algorithm to detect appropriate planes. Nevertheless, after reconstruction, the algorithm generated simplified volumes and small, tower-like structures that do not correspond to the real geometry of these elements. Figure 10 illustrates the representation obtained for the tanks in the model, together with the elevation profile derived from the lidar point cloud in the surroundings of these structures.

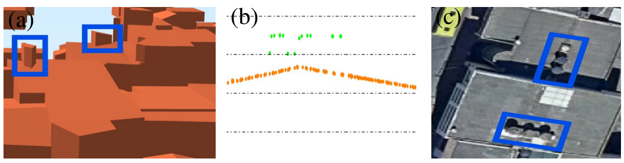

Figure 10. Tank reconstruction. (a) 3D model with tanks; (b) lidar profile; (c) reference image.

As a result of the iterative process, which included more than 40 test configurations, a workflow was developed that integrates the key stages, decision points, and parameter adjustments influencing reconstruction quality, enabling the systematic mitigation of the critical factors affecting LoD2 reconstruction. The workflow was intentionally developed within a controlled study area to facilitate the detailed identification and evaluation of reconstruction failures before being replicated in larger study areas. Designed based on Suter et al. (2026), the workflow adopts a dynamic and iterative approach, where tasks are cyclically refined based on results, enabling progressive optimization of the process. The complete workflow is available in *GitHub repository*.

4. Discussion

This research demonstrates that the geometric and topological consistency of s3DCMs depends on the interaction among input data quality, algorithm parameterization, and the characteristics of the urban environment. Most of the critical factors identified result from limitations in the available geospatial data and the morphological characteristics of the study area. In this context, Roofer was used as an experimental platform to systematically analyze the influence of these factors and assess the extent to which their effects can be mitigated through parameter optimization. However, some limitations—such as the reconstruction of parapets, water tanks, and buildings with multiple base elevations on steep terrain—could not be fully resolved and represent general challenges of reconstruction in mountainous urban environments, rather than limitations unique to Roofer.

The results confirm that the geometric and positional quality of building footprints is critical for reconstruction, as errors can degrade model quality and even halt algorithm execution. Geometric validation of footprints is therefore essential to ensure reliable models, as also highlighted by Chajaei and Bagheri (2025), who showed that poor footprint segmentation introduces biases in morphological indicators. Furthermore, the behavior of critical factor 3 can be explained by the internal boundaries of buildings, which reduce the presence of nearby ground points, thereby affecting the estimation of Z_0.

Lidar point-cloud classification directly influences geometric accuracy and topological consistency; the refinements applied here yielded simultaneous improvements in the metrics (see table 4). This reduction confirms that correctly identifying points is crucial for plane detection and consistency. Park and Guldmann (2019) similarly indicate that unclassified points within footprints introduce biased height estimates caused by incorrect returns on the roof surface, misalignment, and edge ambiguities. These errors, highlight the need for accurate lidar classification to ensure vertical accuracy and geometric consistency in s3DCM. Furthermore, Pađen et al. (2024) emphasize Roofer's sensitivity to quality and alignment of input data, and propose optimized strategies for planar segmentation and handling missing data.

Likewise, the results show that physical factors, such as the interaction of the lidar signal with translucent materials, introduce systematic reconstruction errors (Siddiqui et al., 2016), requiring targeted preprocessing. In addition, estimating the Z_0 on sloped terrain has limitations; although reducing the buffer improves the approximation, it remains constrained by the high variability of the terrain. This limitation is inherent to the terrain itself, given that on sloped sites with terraced buildings, multiple base levels coexist that cannot be represented by a single value of Z_0.

Furthermore, the presence of vegetation indicates that rooftop point availability is more important than overall point-cloud density, since building reconstruction is limited in areas affected by occlusion. This behavior highlights the usefulness of minimum density thresholds to ensure reconstruction, particularly in areas with vegetation. A higher number of points allows more accurate delineation of building shape and structure, whereas low density can hinder reconstruction and affect the representation of complex or decorative details (Kulawiak, 2022; Liu et al., 2024).

Local construction features such as tanks and parapets pose significant challenges because they introduce geometric noise and biases in surface estimation (Giannelli, 2021). Although filtering strategies can improve model consistency, these elements must be preserved in applications such as solar potential analysis due to their impact on shading. Common in Colombian urban contexts, they are often not captured by plane-based reconstruction methods such as Roofer because of their small size, low point density, and classification limitations. This highlights the need to integrate additional semantic information or to adopt hybrid approaches to improve 3D model fidelity. Similarly, features such as balconies and overhangs cannot be reconstructed reliably, as 2.5D-based approaches produce simplified models with flat roofs and vertical walls, omitting protruding elements that cannot be captured with aerial lidar (Pađen et al., 2024).

Taken together, these results demonstrate that 3D urban reconstruction is not exclusively a geometric problem, but rather a broader process that depends on the quality, consistency, and interpretation of multiple information sources. In this regard, generating consistent models requires not only robust algorithms but also methodological strategies tailored to local conditions. Although models may satisfy topological and geometric consistency checks, they often fail to accurately represent the built environment, emphasizing the need for validation approaches that balance geometric rigor with real-world fidelity.

5. Conclusions

The results show that LoD2 reconstruction is highly sensitive to the interaction between input data quality, algorithm parameterization, and the physical characteristics of the urban environment. Rather than representing isolated technical issues, the identified factors describe recurrent conditions associated with official geospatial datasets and heterogeneous urban morphologies. Building footprint quality and lidar classification proved to be the most influential factors because they directly affect both the geometric validity and topological consistency of the reconstructed models. Other limitations, including stepped buildings, vegetation occlusion, and rooftop structures, highlight current challenges for automatic LoD2 reconstruction that cannot always be resolved through parameter optimization alone.

These findings highlight the need for holistic LoD2 reconstruction workflows that integrate rigorous preprocessing, algorithm optimization, and adaptation to local conditions. The main contribution of this study lies not only in identifying these critical factors, but also in developing a reproducible workflow that formalizes the preprocessing stages, decision points, and mitigation strategies required to generate consistent models from the official geospatial datasets available in Colombia, while accounting for the country's mountainous topography, heterogeneous urban morphology, and the inherent limitations of these datasets. Consequently, the proposed workflow provides a practical methodological guide for future LoD2 reconstruction projects in Colombia and other urban environments with similar geographical conditions and geospatial data sources. Future work will evaluate how these reconstruction improvements influence rooftop solar potential estimation within Urban Digital Twin applications.

References

Alvi, M., Dutta, H., Minerva, R., Crespi, N., Raza, S. M., Herath, M., 2025. Global perspectives on digital twin smart cities: Innovations, challenges, and pathways to a sustainable urban future. *Sustainable Cities and Society*, 126, 106356. doi.org/10.1016/J.SCS.2025.106356.

Biljecki, F., Ledoux, H., Du, X., Stoter, J., Soon, K. H., Khoo, V. H. S., 2016. The most common geometric and semantic errors in CITYGML datasets. *ISPRS Annals of the Photogrammetry, Remote Sensing and Spatial Information Sciences*, IV-2/W1, 13–22. doi.org/10.5194/isprs-annals-IV-2-W1-13-2016.

Bing-Shiuan, T., 2024. 3DCityDB-Tools plug-in for QGIS: Adding server-side support to 3DCityDB v.5.0. https://repository.tudelft.nl/file/File_d53d0b95-50ab-4dab-a458-1ea808f66035?preview=1.

Chajaei, F., Bagheri, H., 2025. LOD1 3D city model from LiDAR: The impact of segmentation accuracy on quality of urban 3D modeling and morphology extraction. *Remote Sensing Applications: Society and Environment*, 38, 101534. doi.org/10.1016/j.rsase.2025.101534.

Geniet, F., Séguin, E., Le Bihan, E., Duan, L., Girard, N., Peters, R., Vallet, B., 2025. A new benchmark on LoD 2 building reconstruction from aerial lidar and footprints. *The International Archives of the Photogrammetry, Remote Sensing and Spatial Information Sciences*, XLVIII-1/W6-2025, 83–90. doi.org/10.5194/isprs-archives-xlviii-1-w6-2025-83-2025.

Giannelli, D., 2021. Solar analysis on buildings of favelas in são paulo to estimate PV potential. Master's thesis, Delft University of Technology. https://repository.tudelft.nl/record/uuid:05ff635a-8113-4d65-aae1-bc0c727831d8.

Gröger, G., Kolbe, T. H., Nagel, C., Häfele, K.-H., 2012. Ogc city geography markup language (citygml) encoding standard. http://www.opengeospatial.org/legal/.

Kukulska, A., Salata, T., Cegielska, K., Szylar, M., 2018. Methodology of evaluation and correction of geometric data topology in QGIS software. *Acta Scientiarum Polonorum Formatio Circumiectus*, 17(1), 115–123. doi.org/10.15576/ASP.FC/2018.17.1.115.

Kulawiak, M., 2022. A Cost-Effective Method for Reconstructing City-Building 3D Models from Sparse Lidar Point Clouds. *Remote Sensing*, 14(5), 1278. doi.org/10.3390/rs14051278.

Ledoux, H., 2018. val3dity: Validation of 3D GIS primitives according to the international standards. *Open Geospatial Data, Software and Standards*, 3(1), 1. doi.org/10.1186/s40965-018-0043-x.

Lei, B., Stouffs, R., Biljecki, F., 2023. Assessing and benchmarking 3D city models. *International Journal of Geographical Information Science*, 37(4), 788–809. doi.org/10.1080/13658816.2022.2140808.

León Sánchez, C. A., 2025. Enhancing Urban Energy Applications through Semantic 3D City Models and Open Data. PhD thesis, Delft University of Technology. https://repository.tudelft.nl.

Liu, Y., Obukhov, A., Wegner, J. D., Schindler, K., 2024. Point2Building: Reconstructing buildings from airborne LiDAR point clouds. *ISPRS Journal of Photogrammetry and Remote Sensing*, 215, 351–368. doi.org/10.1016/j.isprsjprs.2024.07.012.

Luo, J., Liu, P., Xu, W., Zhao, T., Biljecki, F., 2025. A perception-powered urban digital twin to support human-centered urban planning and sustainable city development. *Cities*, 156, 105473. doi.org/10.1016/J.CITIES.2024.105473.

OGC, 2021. Ogc city geography markup language (citygml) conceptual model standard. http://www.opengis.net/doc/IS/CityGML-1/3.0.

Pađen, I., Peters, R., García-Sánchez, C., Ledoux, H., 2024. Automatic high-detailed building reconstruction workflow for urban microscale simulations. *Building and Environment*, 265, 111978. doi.org/10.1016/j.buildenv.2024.111978.

Park, Y., Guldmann, J.-M., 2019. Creating 3D city models with building footprints and LIDAR point cloud classification: A machine learning approach. *Computers, Environment and Urban Systems*, 75, 76–89. doi.org/10.1016/j.compenvurbsys.2019.01.004.

Peters, R., Dukai, B., Vitalis, S., van Liempt, J., Stoter, J., 2022. Automated 3D Reconstruction of LoD2 and LoD1 Models for All 10 Million Buildings of the Netherlands. *Photogrammetric Engineering & Remote Sensing*, 88(3), 165–170. doi.org/10.14358/PERS.21-00032R2.

Siddiqui, F., Teng, S., Awrangjeb, M., Lu, G., 2016. A Robust Gradient Based Method for Building Extraction from LiDAR and Photogrammetric Imagery. *Sensors*, 16(7), 1110. doi.org/10.3390/s16071110.

Suter, F., Coleman, T., Altintaş, İ., Badia, R. M., Balis, B., Chard, K., Colonnelli, I., Deelman, E., Di Tommaso, P., Fahringer, T., Goble, C., Jha, S., Katz, D. S., Köster, J., Leser, U., Mehta, K., Oliver, H., Peterson, J.-L., Pizzi, G., Ferreira da Silva, R., 2026. A terminology for scientific workflow systems. *Future Generation Computer Systems*, 174, 107974. doi.org/10.1016/j.future.2025.107974.

Taha, A. A., Hanbury, A., 2015. An Efficient Algorithm for Calculating the Exact Hausdorff Distance. *IEEE Transactions on Pattern Analysis and Machine Intelligence*, 37(11), 2153-2163. doi.org/10.1109/TPAMI.2015.2408351.

Wysocki, O., Schwab, B., Beil, C., Holst, C., Kolbe, T. H., 2024. Reviewing Open Data Semantic 3D City Models to Develop Novel 3D Reconstruction Methods. *International Archives of the Photogrammetry, Remote Sensing and Spatial Information Sciences*, XLVIII-4-2024, 493–500. doi.org/10.5194/isprs-archives-XLVIII-4-2024-493-2024.

Zhou, D., Fang, J., Song, X., Guan, C., Yin, J., Dai, Y., Yang, R., 2019. IoU loss for 2d/3d object detection. *Proceedings of the IEEE International Conference on 3D Vision (3DV)*, 85–94. https://doi.org/10.1109/3DV.2019.00019.